Supporting Information

A Design Strategy of High-Activity Swarm Mobile Nanocatalysts for Hydrogenolysis of Complex N-Benzyl Compounds via Anchoring-Confinement Synergy

Junjie Wang,[a] Yuanyuan Ma,[a] Jianwei Song,[b] Chuanyou Xiao,[b] He Huang,[a] Chenghui Sun,*[a] and Siping Pang*[a]

a. School of Materials Science & Engineering, Beijing Institute of Technology, Beijing 100081, China

b. Qing Yang Chemical Industry Corporation, Liaoyang 111001, China

*** Corresponding author:**

Chenghui Sun: sunch@bit.edu.cn

Siping Pang: pangsp@bit.edu.cn

SUPPORTING FIGURES AND TABLES

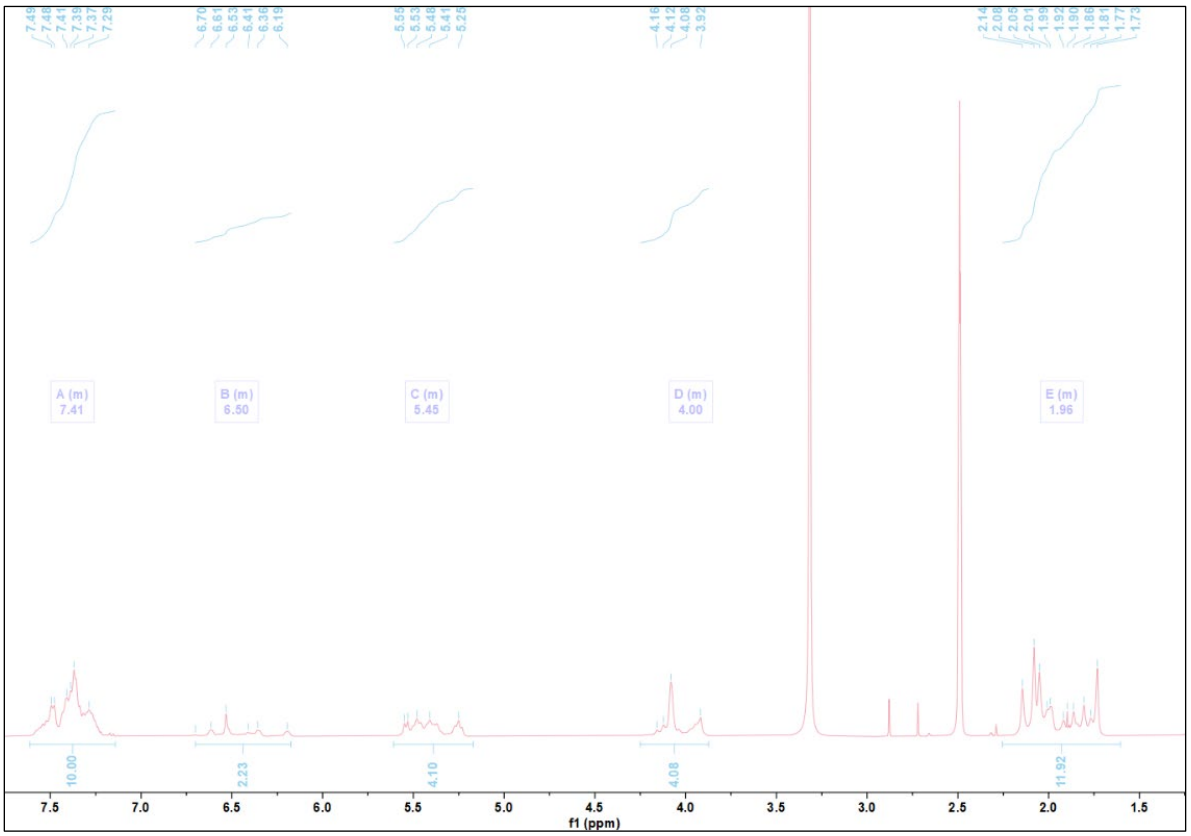

Fig. S1. ^{1}H NMR spectrum for the product TADBIW from HBIW hydrogenolysis (in DMSO).

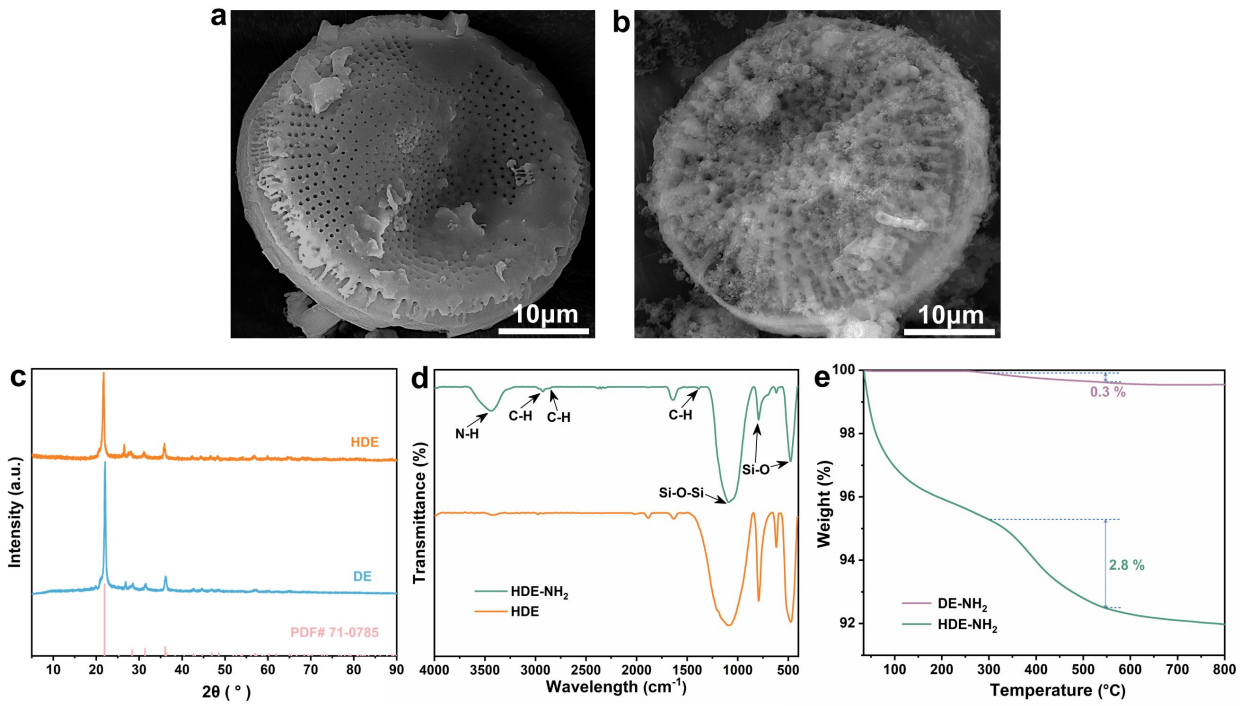

Fig. S2. SEM images of (a) DE and (b) HDE. (c) XRD patterns of DE and HDE. (d) FTIR spectra and (e) TGA curves of the prepared samples.

This observation further confirms that the synthetic conditions employed were sufficiently mild to preserve the morphology (Fig. S2a-c). In the FTIR spectra (Fig. S2d), a characteristic absorption band in the range of 3300-3500 cm^{-1} was observed, which can be attributed to the symmetric and asymmetric stretching vibrations of the $-NH_2$ groups of the alkylamine ($-CH_2CH_2CH_2NH_2$). Additionally, the peaks at 2927 cm^{-1} and 2850 cm^{-1} were associated with the asymmetric and symmetric stretching vibrations of C-H in $-CH_2-$, respectively, and the peak at 1386 cm^{-1} corresponded to the in-plane flexural vibration of C-H, indicating the successful grafting of alkylamine onto the surface of HDE. The sample is henceforth referred to as HDE-NH_2. Furthermore, the peak at 1089 cm^{-1} was assigned to the asymmetric stretching vibration of Si-O-Si, while the peaks at 792 cm^{-1} and 476 cm^{-1} were identified as the symmetric stretching vibration and the flexural vibration of Si-O, respectively, which are characteristic of the HDE itself. TGA

curves indicate a significantly higher number of -NH_2 groups present on the surface of the HDE-NH_2 (Fig. S2e), while also demonstrating the thermal stability of this support.

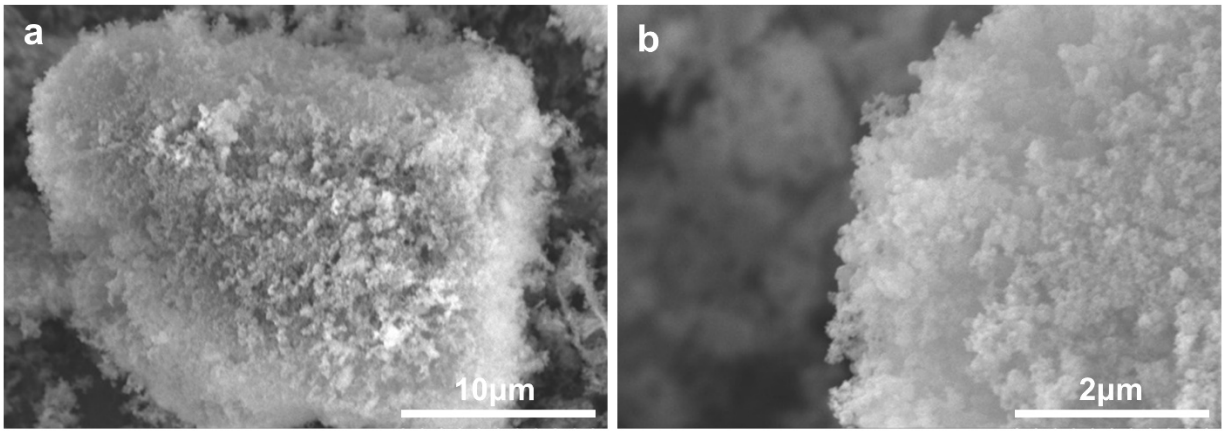

Fig. S3. SEM images of DE using a high concentration of NaOH.

The critical parameter for controlling the desired hierarchical structure is the alkaline concentration in the solution.The solution must possess sufficient basicity to partially dissolve DE, thereby releasing silicate species for the subsequent condensation process. Conversely, if the solution becomes excessively basic, the integrated macroporosity of DE would be compromised, potentially leading to complete dissolution of DE. The phenomenon has been corroborated through a control experiment employing a higher NaOH concentration (Fig. S3).

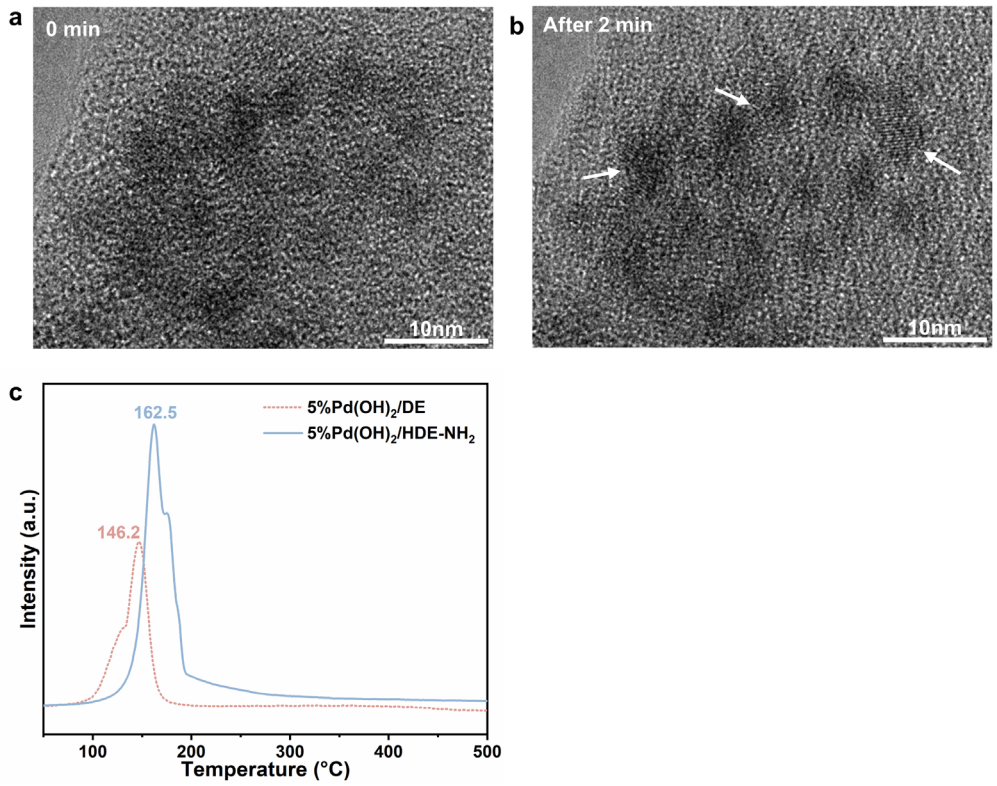

Fig. S4. (a, b) HRTEM images of selected areas over time. (c) H_2-TPR profiles of catalysts.

To substantiate the hypothesis, the same region was subjected to prolonged HRTEM analysis (Fig. S4a, b). Over time, the region displayed increasingly pronounced lattice structures, particularly at locations marked by white arrows. This observation aligns with previous reports in the literature.[1] As shown in Fig. S4c, the highest reduction peak of 5%$Pd(OH)_2$/DE was located at 146.2 °C, but the corresponding peak for 5%$Pd(OH)_2$/HDE-NH_2 was shifted to 162.5 °C. These findings indicated that the Pd species in 5%$Pd(OH)_2$/HDE-NH_2 were more resistant to reduction.

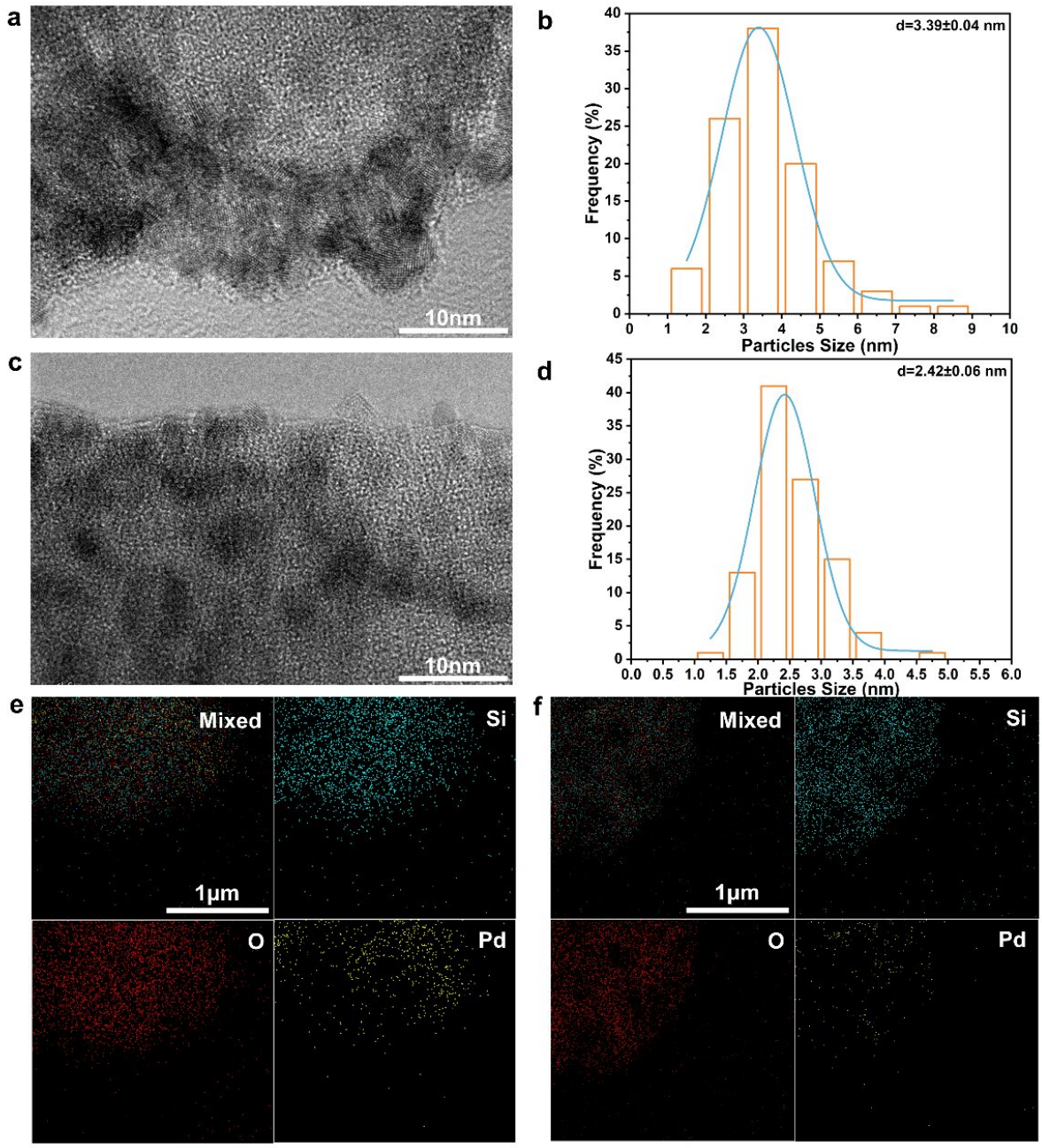

Fig. S5. (a, c) HRTEM images, (b, d) corresponding size distribution histograms, and (e-f) STEM-EDS elemental mappings of 5%$Pd(OH)_2$/DE-NH_2 and 5%$Pd(OH)_2$/HDE, respectively.

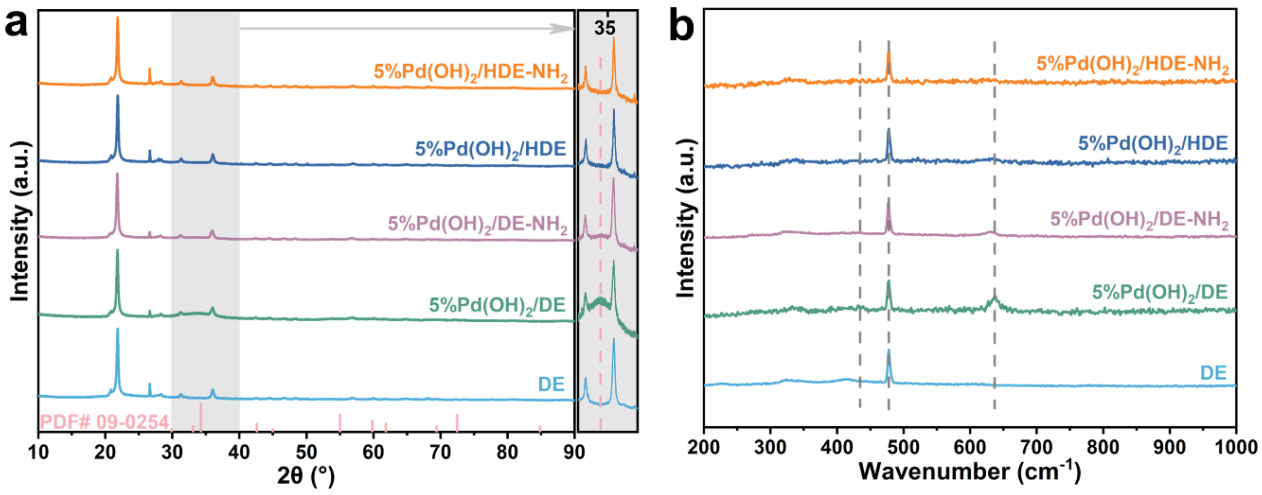

Fig. S6. (a) XRD patterns and (b) Raman spectroscopies of the prepared catalysts.

The frequencies corresponding to the main vibration modes in the silica structure (Si-O-Si) were identified at 478 cm^{-1} (the rocking mode).[2, 3] Additionally, the peaks around 434 cm^{-1} and 640 cm^{-1} were attributed to Pd-O stretching vibrations (Fig. S6b).[4]

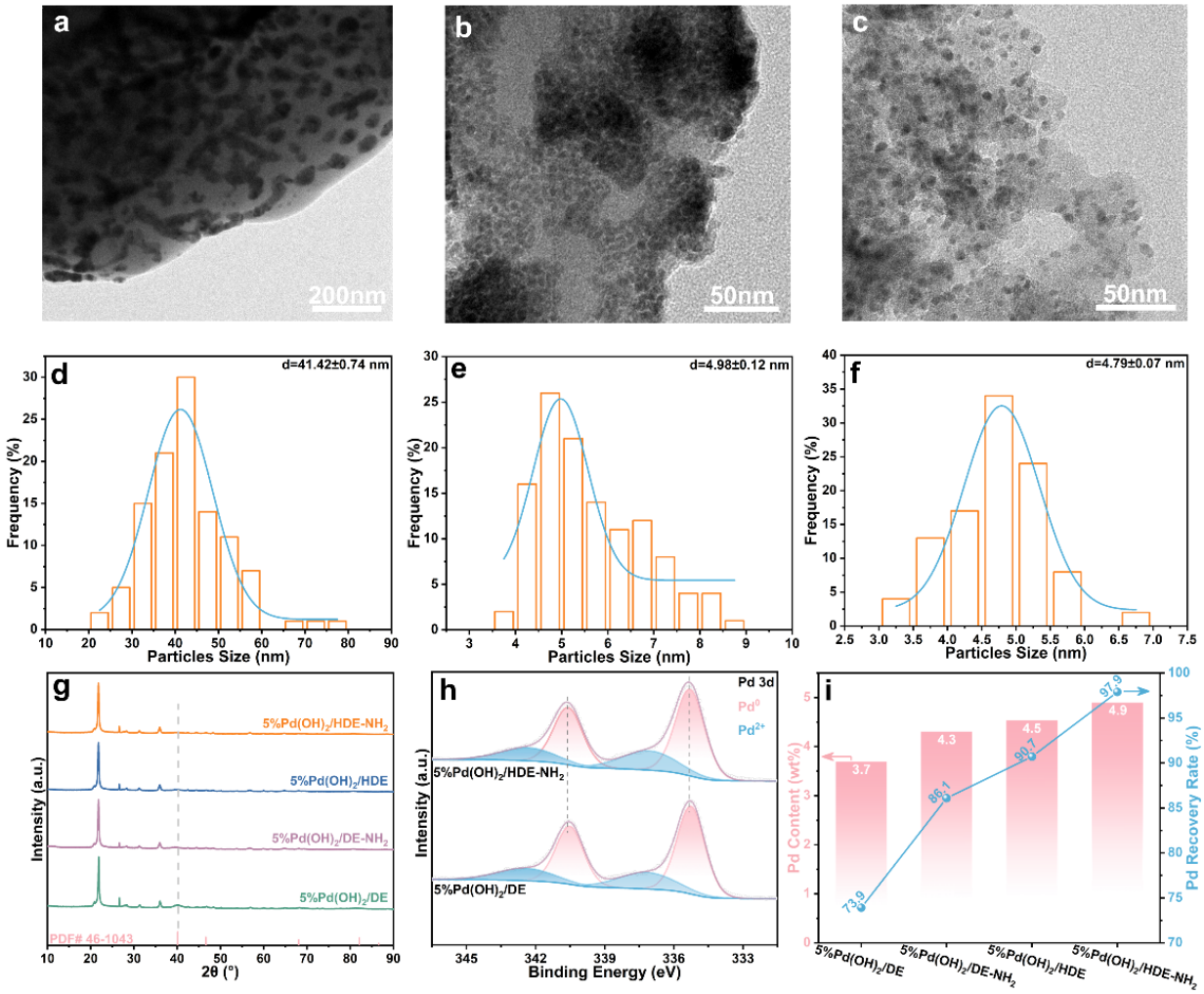

Fig. S7. Morphological and structural characterization of spent catalysts. (a-c) HRTEM images, (d-f) corresponding size distribution histograms of spent 5%$Pd(OH)_2$/DE, 5%$Pd(OH)_2$/DE-NH_2, and 5%$Pd(OH)_2$/HDE. (g) XRD patterns, (h) High-resolution XPS Pd 3d spectra, and (i) ICP-OES of the spent catalysts.

Following HBIW debenzylation, the collection of catalysts is essential for a comprehensive understanding of the reaction mechanism and the recovery of the noble metal palladium. Consequently, the retrieved catalysts were thoroughly characterized using HRTEM, XRD, XPS, and ICP-OES. The leached Pd species were proven to be the sole genuine catalytic intermediates in the reaction, as demonstrated by the swarm mobile catalysis. It was evident that the growth of Pd follows the Ostwald ripening process when the leached Pd species redeposited back onto the

support after the reaction. Ostwald ripening is a process where smaller nanoparticles dissolve and redeposit onto larger nanoparticles. When Pd was deposited onto support surfaces, the dissolved species can travel a short distance to be deposited onto nearby larger nanoparticles. This is the case for 5%$Pd(OH)_2$/DE catalyst. The growth of Pd during the reaction was unrestricted, leading to the large aggregates observed in the spent catalyst (Fig. S7a, d). However, due to the "anchoring-confinement" synergistic induction effect of 5%$Pd(OH)_2$/HDE-NH_2 catalyst, the dissolved Pd species must disengage from the binding of amino groups and travel a much longer distance along the narrow microporous-mesoporous channel before being deposited onto larger nanoparticles. Therefore, particle growth via Ostwald ripening became considerably more challenging in the presence of this effect, mitigating the likelihood of rapid Pd species growth (Fig. 6h). Nonetheless, neither the anchoring effect nor the confinement effect alone can ensure the high dispersion and high density of reloaded Pd, and the Pd species sizes of the two samples also exhibited slight growth (Fig. S7b, c, e, f). Other potential mechanisms (such as direct fusion or aggregation among the Pd nanoparticles) can be excluded, given the low reaction temperature.

Furthermore, the changes in the spent catalysts were detected by XRD (Fig. S7g). It was observed that the $Pd(OH)_2$ diffraction peak at $2\theta=34.26°$ (PDF#09-0254) disappeared in all samples, and the spent 5%$Pd(OH)_2$/DE catalyst at $2\theta=40°$ exhibited an obvious Pd metal diffraction peak (PDF#46-1043).[5] This indicated that $Pd^{\sigma+}$ ($\sigma>0$) gradually transformed into Pd^0 during the reaction, and the broadening peak was attributed to the poor crystallinity of Pd nanoparticles. The absence of evident diffraction peaks in the remaining samples at $2\theta=40°$ was related to the small size or high dispersion of Pd nanoparticles. Significantly, the support retained

its crystalline structure as confirmed by XRD analysis after reaction. This confirmed that the support exhibited outstanding stability.

Moreover, XPS measurements were conducted on the spent 5%$Pd(OH)_2$/DE and spent 5%$Pd(OH)_2$/HDE-NH_2 catalysts to further elucidate the metal-support interaction (MSI) between Pd and the supports. The high-resolution Pd 3d spectra, depicted in Fig. S7h, can be deconvoluted into two main characteristic peaks. The double peaks at approximately 335.3 and 340.6 eV were attributed to Pd^0, while the double peaks at approximately 336.9 and 342.2 eV were associated with Pd^{2+}. Based on the XPS data, Pd^0 was the predominant valence state on the surface of the spent catalysts. Notably, compared to the spent 5%$Pd(OH)_2$/DE, the Pd 3d (metal) peaks of the spent 5%$Pd(OH)_2$/HDE-NH_2 shifted to a higher binding energy, indicating an increased valence state of Pd. Consequently, the stronger MSI between Pd atoms and the support in the spent 5%$Pd(OH)_2$/HDE-NH_2.[6, 7]

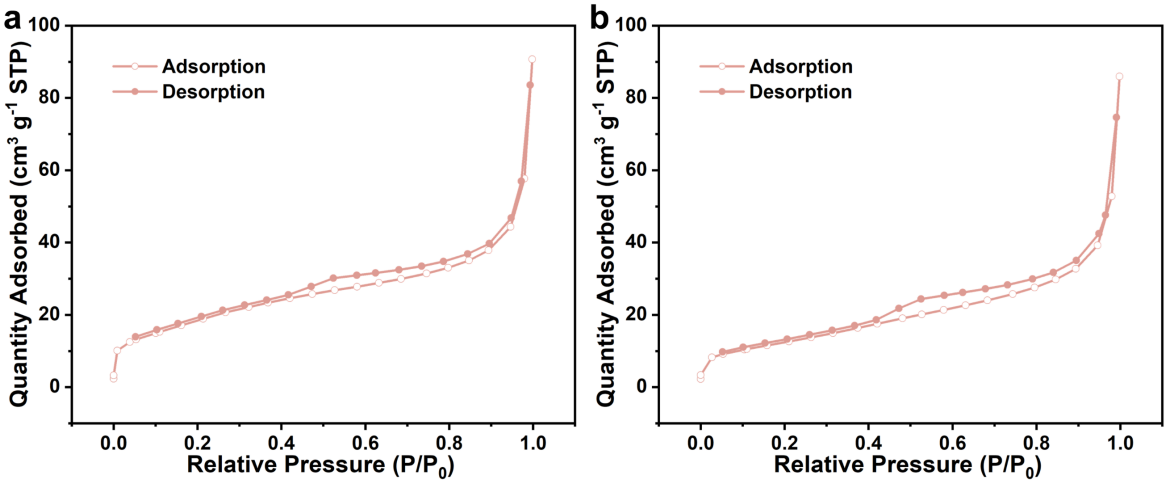

Fig. S8. N_2 adsorption-desorption isotherms of the catalyst (a) before, and (b) after the hydrogenation.

To evaluate the textural properties of the catalyst after the hydrogenation reaction, we conducted BET analysis Fig. S8 Before and after the hydrogenolysis reaction, there were no significant changes in the isotherms of the catalyst, with only a slight decrease observed at low P/P_0. Furthermore, the results indicated a slight decrease in the BET surface area compared to the fresh catalyst, from 97.2 m^2/g to 94.9 m^2/g. This minor reduction was likely due to the adsorption of reaction byproducts or partial pore blockage during the reaction.

Table S1 The metal dispersion and active particle diameter of samples

Sample	Metal dispersion (%)	Active particle diameter (nm)
5%$Pd(OH)_2$/DE	37.6	5.5
5%$Pd(OH)_2$/DE-NH_2	42.8	3.1
5%$Pd(OH)_2$/HDE	47.6	2.3
5%$Pd(OH)_2$/HDE-NH_2	51.0	1.8

SUPPORTING REFERENCES

1 X. Cao, Z. Chen, R. Lin, W. C. Cheong, S. Liu, J. Zhang, Q. Peng, C. Chen, T. Han and X. Tong, *Nat. Catal.*, 2018, **1**, 704-710.

2 K. J. Kingma and R. J. Hemley, *Am. Mineral.*, 1994, **79**, 269-273.

3 I. Petreanu, V. C. Niculescu, S. Enache, C. Iacob and M. Teodorescu, *Anal. Lett.*, 2023, **56**, 390-403.

4 H. Zhang, C. Wang, H. L. Sun, G. Fu, S. Chen, Y. J. Zhang, B. H. Chen, J. R. Anema, Z. L. Yang and J. F. Li, *Nat. Commun.*, 2017, **8**, 15447.

5 F. Xue, Q. Li, M. Lv, Y. Song, T. Yang, X. Wang, T. Li, Y. Ren, K. Ohara and Y. He, *J. Am. Chem. Soc.*, 2023, **145**, 26728-26735.

6 H. Zhao, C. Liu, Y. Zheng, S. Li, Y. Gao, Q. Ma, F. Wang and Z. Dong, *ACS Catal.*, 2024, **14**, 8619-8630.

7 Y. Wang, G. Wang, L. I. van der Wal, K. Cheng, Q. Zhang, K. P. de Jong and Y. Wang, *Angew. Chem.*, 2021, **133**, 17876-17884.